Using Covariance Matrix and Fast Fourier Transform for Estimating Spectrum Hole Location in Cognitive Radio Network

[1]EMESHILI O. JOSEPH   [2]EMMANUEL ERONU   [3]EVANS ASHIGWUIKE
[123]Department of Electrical/Electronics Engineering, University of Abuja
NIGERIA

Abstract: This paper worked on Using Covariance Matrix and Fast Fourier Transform for Estimating Spectrum Hole Location in Cognitive Radio Network, Fast Fourier Transform (FFT) was used to split the Spectrum into sub-band channels. The paper adopted the use of Covariance Matrix in determining the actual range for the bounds. From the result it can be deduce that the areas where there are no signals at all are point where noise is prevalent, while thee point between 0 and 20 on the principal component axis are the point where you have high possibility of spectrum hole availability, the point between 20 and 30 on the principal axis is the point with high possibility of error false alarm.. Fast Fourier Transform was used to decompose the wideband spectrum to 64 Sub-band channels. the result of this shows that there exists a relationship between the covariance matrix and the sub-band energy. Two important properties of any square matrix are its trace, and its determinant. Analysis of Results obtained from Simulations shows that at signal-to-noise ratio (SNR) value of -10dB, spectrum holes were identified in 2 sub-band channels 13 and 53.

Key-Words: -Fast Fourier Transform, Covariance Matrix, Cognitive Radio, Spectrum, Ultra-Wide Band

1 Introduction

The recent increase in the demand for the already scarce wireless radio bandwidth has added weight to the increase in scarcity of radio spectrum. A recent study by Cisco [1] showed that global mobile data traffic grew by 71 percent in 2017 alone, reaching 11.5 exabytes per month of that year. The same study showed that nearly 650 million devices and connections were added in 2017. Another contributing factor to the problem of spectrum scarcity is the nature of spectrum allocation implemented by regulatory agencies, which causes inefficient utilization of radio spectrum [2]. Given a wideband spectrum range, as shown in Figure 1 [3], a scan reveals some bands are vacant, some bands are sparingly utilized, and others are entirely used.[[15][16]
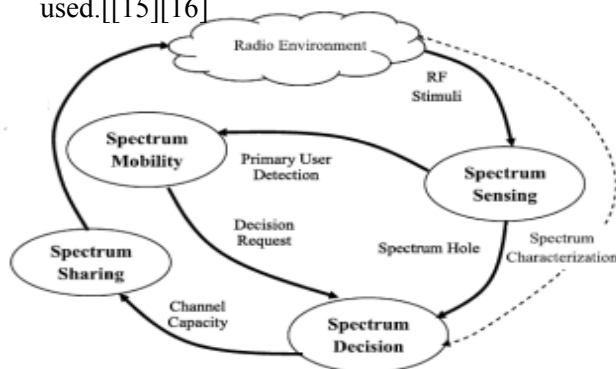

Figure 1 **Cognitive cycle of cognitive radio [6]**

Cognitive Radio is an emerging technique to increase the effective usage of the spectrum. Due to the rapid development in number of wireless devices and gadgets, there is a scarcity in radio frequency band. This lead to the spectrum sensing concept of identifying the unused spectrum holes. Spectrum sensing can be defined as the ability to detect the presence or absence of a licensed user in the channel, while the most challenging task is to sense in very low SNR regime [2][13]

ınications over a large portion of the radio spectrum

The ultrawide band signal shown in Figure 1 is the concatenation of different signals with varying frequencies.[4][12][13]

The signal was generated using the relationship in equation (1).

A range of frequencies are depicted in the equation spread through the spectrum shown in the relationship in equation 1

$$x(t) = x_1(t) + x_2(t) + x_3(t) + x_4(t) + x_5(t) + x_6(t) + x_7(t) + x_8(t) + x_9(t) + x_{10}(t) + x_{11}(t)$$

$$(1)$$

between time and frequency)in equation 1 and fig 1.

The signal in fig 1 and 2 are wideband signal embed with noise , signal which the frequency increases linearly over time [3][14]
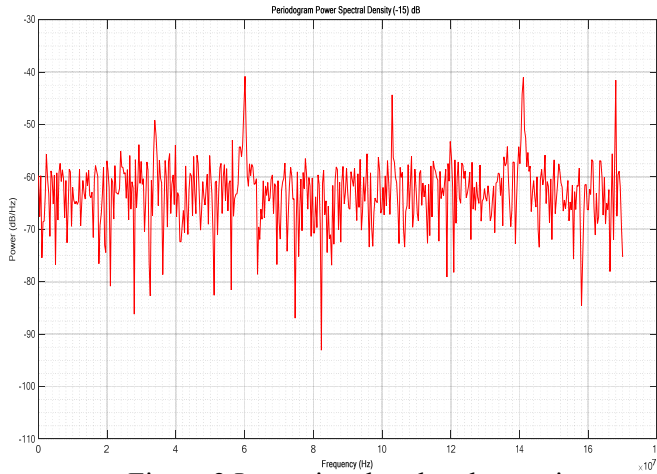

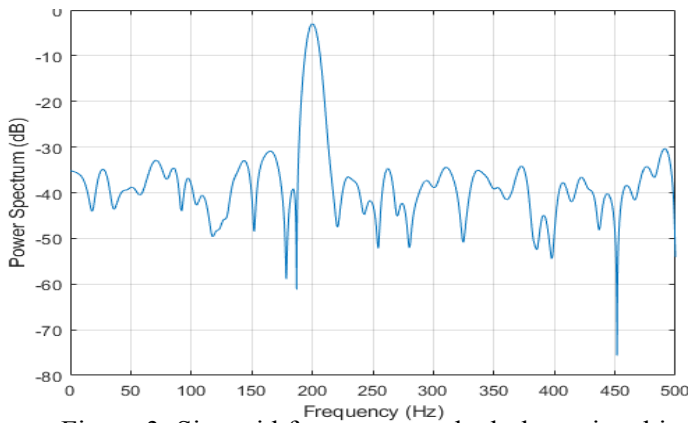Figure 2 Input signal under observation

Figure 3 Sinusoid frequency embed the signal in white Gaussian noise

2. Filter Bank using Fast Fourier Transform

The diagram in Fig 4 is the decomposed signal using an FFT (Fast Fourier transform) filter bank is shown in Fig 5 where the signals in each channel of the filter bank are.[3][15]
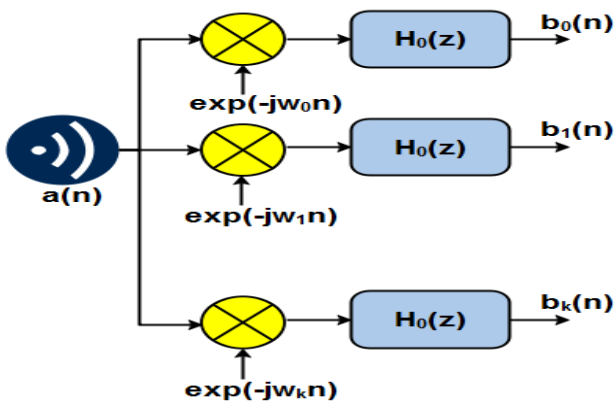

Figure 4 The signal decomposition using an FFT (fast Fourier transform)

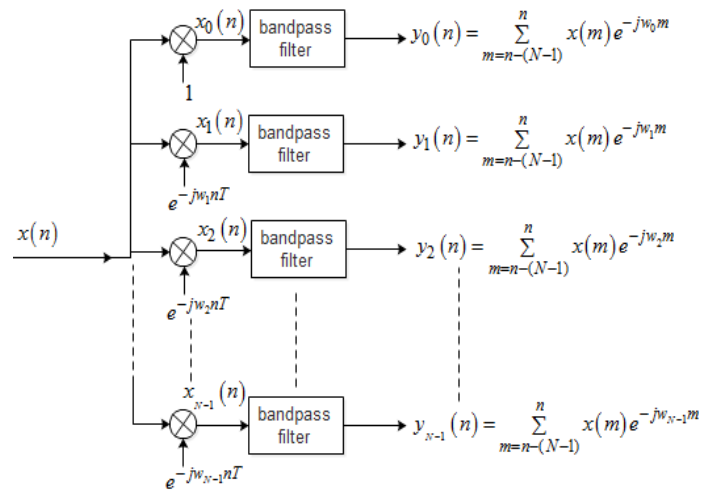This also shown in figure 5 and 6 which was

Figure 5 FFT Splitting of Wideband Signal

computed using an exponential function with varying frequencies computed using an exponential function with varying frequencies.
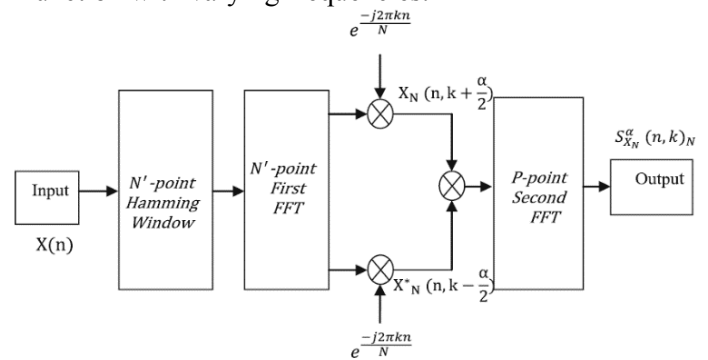

Figure 6 Fast Fourier Transform Accumulation Method

In this work considered splitting channels from channel 1 to Channel k shown in equation 2 and equation 3, the FFT filter bank considered has 64 sub-band channels. Thus, the first sub-band channel for the FFT filter bank in Fig 4 has an index of 1, while the last sub-band channel has an index of 64. With this arrangement, the decomposition of the input signal shown by the filter bank shown in Figure 4 will yield an array of coefficients spread across 64 sub-band channels as shown in Figure 7. The coefficients in each sub-band channel are computed using the relationships defined in equations.[4][15][6]

$$channel_0 = b_0(n) = \sum_{m=n-(N-1)}^{n} a(m)e^{-jw_0 m}$$

$$channel_1 = b_1(n) = \sum_{m=n-(N-1)}^{n} a(m)e^{-jw_1 m}$$

$$\vdots$$

$$channel_k = b_k(n) = \sum_{m=n-(N-1)}^{n} a(m)e^{-jw_k m}$$

$$\dots\dots(2)$$

$$x_1(t) = A_1 \sin(2\pi f_1 t)$$
$$x_2(t) = A_2 \sin(2\pi f_2 t)$$
$$x_3(t) = A_3 \sin\left[\phi_{3_0} + 2\pi\left(f_{3_0}t + \frac{k_3}{2}t^2\right)\right], \phi_{3_0} = 0, k_3 = \frac{f_{3_1} - f_{3_0}}{T_3}$$
$$x_4(t) = A_4 \sin(2\pi f_4 t)$$
$$x_5(t) = A_5 \sin\left[\phi_{5_0} + 2\pi\left(f_{5_0}t + \frac{k_5}{2}t^2\right)\right], \phi_{5_0} = 0, k_5 = \frac{f_{5_1} - f_{5_0}}{T_5}$$
$$x_6(t) = A_6 \sin(2\pi f_6 t)$$
$$x_7(t) = A_7 \sin(2\pi f_7 t)$$
$$x_8(t) = A_8 \sin\left[\phi_{8_0} + 2\pi\left(f_{8_0}t + \frac{k_8}{2}t^2\right)\right], \phi_{8_0} = 0, k_8 = \frac{f_{8_1} - f_{8_0}}{T_8}$$
$$x_9(t) = A_9 \sin(2\pi f_9 t)$$
$$x_{10}(t) = A_{10} \sin(2\pi f_{10} t)$$
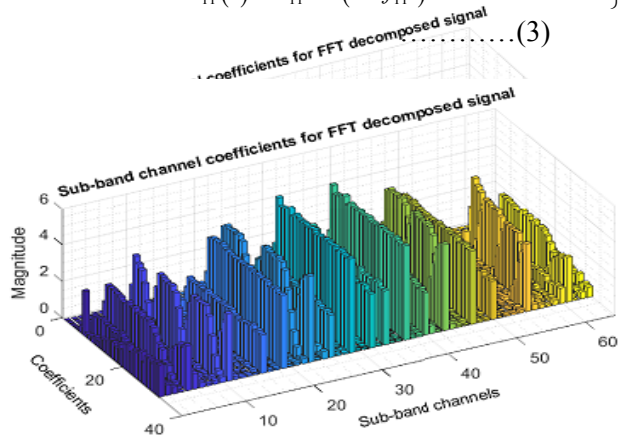$$x_{11}(t) = A_{11} \sin(2\pi f_{11} t)$$

$$\dots\dots\dots(3)$$

Figure 7 The signal decomposition using an FFT (fast Fourier transform)

3 Cyclostationary Detection

Cyclostationary detection is a technique that deals with the periodicity of periodic signals using FFT. This technique, as described in [7], uses spectral correlation function to detect the periodicity of the signal from the primary user. The cyclostationary detector shown in Figure 8 exploits sinusoidal carriers, pulse trains, spreading code and other features in the detection of the periodicity.[16][18][19]

Figure 8: Cyclostationary Detection

For a received signal [17], the cyclic spectral density (CSD) function is:

$$S(f,\alpha) = \sum_{\tau=\infty}^{\infty} R_y^\alpha(\tau)e^{-j2\pi f\tau} \qquad \text{where}$$

$$R_y^\alpha(\tau) = E\left[y(n+\tau)y^*(n-\tau)e^{j2\pi\alpha n}\right] \quad \dots(4)$$

The equation is the cyclic autocorrelation function, and the cyclic frequency is α. The cyclic spectral density function gives a maximum output at points where the fundamental frequencies of the received signal are equal to the cyclic frequency. [18][20]

4 Cyclic Spectrum Estimation

Communication systems are increasingly developed in a discrete domain employing digital conversion. In practice, cyclic spectrum estimation can be done using two algorithms, the FFT accumulation method (FAM) and Strip Spectral Correlation Analyzer (SSCA). In [12], authors discuss in detail different approaches of the two estimation methods: in the time domain and frequential domain. These two methods are based on changes in the smoothed cyclic cross periodogram which is defined as

$$\int_{xyT}^{\alpha}(n,f) = \lim\frac{1}{2n+1}\sum_{n=-N}^{N}\frac{1}{T}X_T\left(n,f+\frac{\alpha}{2}\right)Y_T^*\left(n,f-\frac{\alpha}{2}\right)\dots\dots\dots(5)$$

$$\int_{xyT}^{\alpha}(n,f) = \lim\frac{1}{2n+1}\sum_{n=-N}^{N}\frac{1}{T}X_T\left(n,f+\frac{\alpha}{2}\right)Y_T^*\left(n,f-\frac{\alpha}{2}\right)$$

where

$$\int_{xyT}^{\alpha}(n,f) = \lim\frac{1}{2n+1}\sum_{n=-N}^{N}\frac{1}{T}X_T\left(n,f+\frac{\alpha}{2}\right)Y_T^*\left(n,f-\frac{\alpha}{2}\right)$$

and are the complex envelopes of the signal x(n) and y(n) respectively and which are calculated as follows,

$$R_{xx}^\alpha = \lim_{T\to\infty}\frac{1}{T}\int_{\frac{T}{2}}^{\frac{T}{2}} R_{xx}(t,\tau)e^{-i2\pi\alpha t}dt\dots\dots(6)$$

Below is a 3 D representation of a two sided display of the spectrogram as a waterfall plot.[8][9] The information here shows a break down in 2 domains both frequency and time. The figure 5 gives a clear
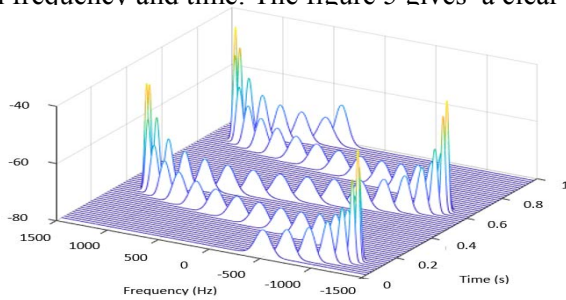

Figure 9 visualisation of how the Signal is

visualisation of how the graph is represented[6]

Considering the FFT in equation 1 for each of the 64 sub-band channels, a covariance matrix is generated from the reduced principal components using the relationship in (2)][7]:

5 Covariance Matrix

Covariance Matrix is used in specifically detecting hole location in the spectrum , this is after all the convergence has been realised. Employing a Power spectral Density map (PSD), the general representation of a covariance is given in equation 7 below

$$Covariance(x, y) = \frac{1}{n}\sum_{i=1}^{n}(x_i - \bar{x})(y_i)\ldots\ldots7$$

* ❖ $Covariance(x, x)\ of\ spectrum\ data = var(x)$
* ❖ $Covariance(x, y) = Covariance(y, x)$
* ❖ Let's assume a spectral Data plot in figure 10 note that y axis represent the Energy level while the x axis represent the frequency. [10]
* ❖ The plot in figure 11 show a scattered graph of spectrum data, this platform will make it possible for covariance method to locate a point with high possibility of a spectrum hole.[11][21]
  Covariance method is shown in equation 7
  * ❖ $Covariance(x, x) = var(x)$
  * ❖ $Covariance(x, y) = Covariance(y, x)$
  * ❖ Let's assume a spectral Data plot in figure 10 note that y axis represents the Energy level while the x axis represent the frequency.
  * ❖ The plot in figure 11 show a scattered graph of spectrum data, this platform will make it

possible for covariance method to locate a point with high possibility of a spectrum hole.

Covariance method is shown in equation 8
$$Covariance(x, y) = \frac{1}{n}\sum_{i=1}^{n}(x_i - \bar{x})(y_i - \bar{y})..8$$

* • Diagonization will help further reduce the data using covariance matrix, there is high possibility of hole detection in the data within the diagonal of the matrix

$$Cov\ (\textstyle\sum)$$
$$= \begin{bmatrix} cov(x_1, x_1) & cov(x_1, x_2) & \cdots & cov(x_1, x_m) \\ cov(x_2, x_1) & cov(x_2, x_2) & \cdots & cov(x_2, x_m) \\ \vdots & \vdots & \vdots & \vdots \\ cov(x_m, x_1) & cov(x_m, x_2) & \cdots & cov(x_m, x_m) \end{bmatrix}$$

$$Cov\ (\textstyle\sum) = \frac{1}{n}(X - \bar{X})(X - \bar{X})^T; where\ X \begin{bmatrix} x_1 \\ x_2 \\ \vdots \\ x_m \end{bmatrix}$$

```
c = randn(5,5)
c =
  0.5377  -1.3077  -1.3499  -0.2050   0.6715
  1.8339  -0.4336   3.0349  -0.1241  -1.2075
 -2.2588   0.3426   0.7254   1.4897   0.7172
  0.8622   3.5784  -0.0631   1.4090   1.6302
  0.3188   2.7694   0.7147   1.4172   0.4889
>>  a_cov = a * a'
Undefined function or variable 'a'.
 >> cov = a * a'
Undefined function or variable 'a'.
 >>  c_cov = c * c'
c_cov =
  4.3142  -3.3292  -2.4655  -3.3249  -4.3772
 -3.3292  14.2353  -3.1405  -2.3052   0.7867
 -2.4655  -3.1405   8.4796   2.5011   3.2092
 -3.3249  -2.3052   2.5011  18.1953  12.9338
 -4.3772   0.7867   3.2092  12.9338  10.5297
```
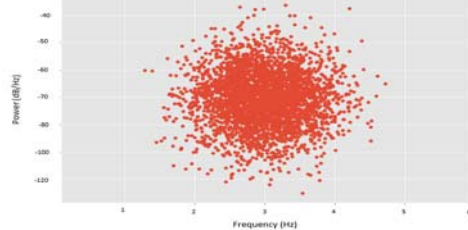

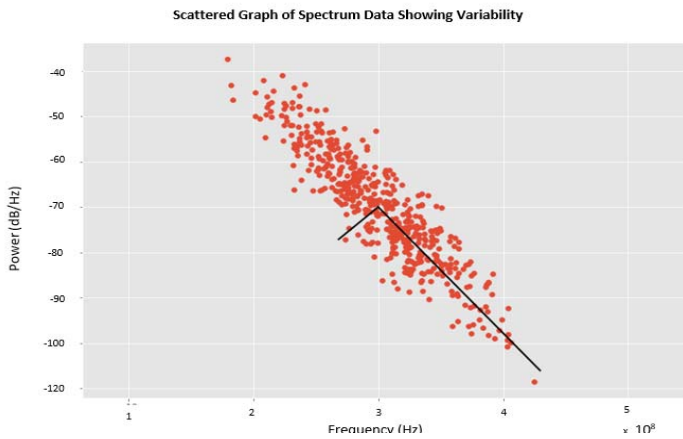Figure 10. PCA Graph of Spectrum Data with reduced noise

Figure 11. Test for Variability

From the covariant matrix generated the diagonal elements generated is most likely the location where the spectrum hole is most likely to be , the significance of the covariance is that the noise associate with spectrum is first reduced to a minimal level there after making it possible to possible approximations and estimation on the spectrum hole location. The graph in figure 12 shows the denoising process carried out.
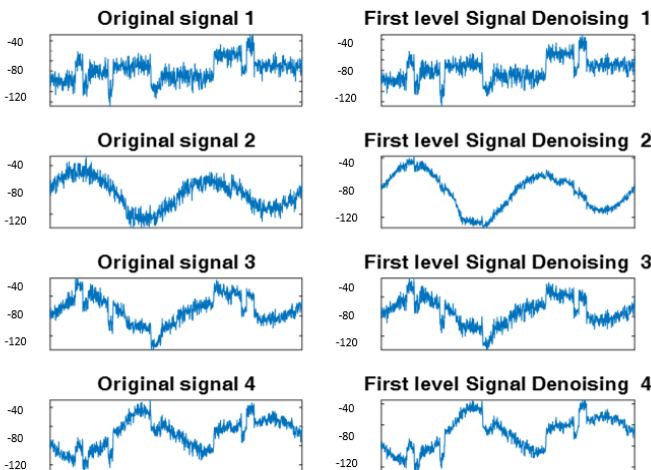

Figure 12 Data Denoising Technique

The covariance matrices generated   are square matrices, and each of them is assigned to a slice in a tensor.

$$\mathbf{R_z} = \frac{1}{N-1}\mathbf{z}\mathbf{z}^\mathbf{T} \qquad (9)$$

The elements $\mathbf{a_1},..,\mathbf{a_n}$ in used in the computation of the principal component, are also used in the computation of the energy of each sub-band channel in Figure 4 using the relationship:[4]

$$E(a_i) = \sum_{n=0}^{N-1} |(a_i)|^2 \qquad\dots\dots\dots\dots(10)$$

The covariance matrix in equation (9) is related to the elements $\mathbf{a_1},..,\mathbf{a_n}$. Two important properties of any square matrix are its trace, and its determinant.

The trace of the covariance matrix in (11) was computed using the relationship:[11]

$$Trace(\mathbf{R_z}) = \sum_{i=1}^{n} z_{ii}$$

$$(11)$$

A comparison between the results obtained reveals that the energy in a sub-band channel and the trace of the covariance matrix generated from its principal components are related by the following relationship:[12]

$$E(a_i) \approx \alpha\left[Trace(\mathbf{R_z})\right] \qquad (12)$$

$$ratio = \frac{1}{length\left[Trace(\mathbf{Rz})_1\right] \vee length\left[E(\mathbf{a}_1)\right]}\sum_{i=1}^{N}\frac{Trace(\mathbf{R_z})_i}{E(\mathbf{a}_i)}$$

$$\dots\dots\dots\dots(13)$$

where $\alpha > 1$ is a scaling factor. A simulation based on the relationships in (11) and (12) yields the results shown in Figure 13.
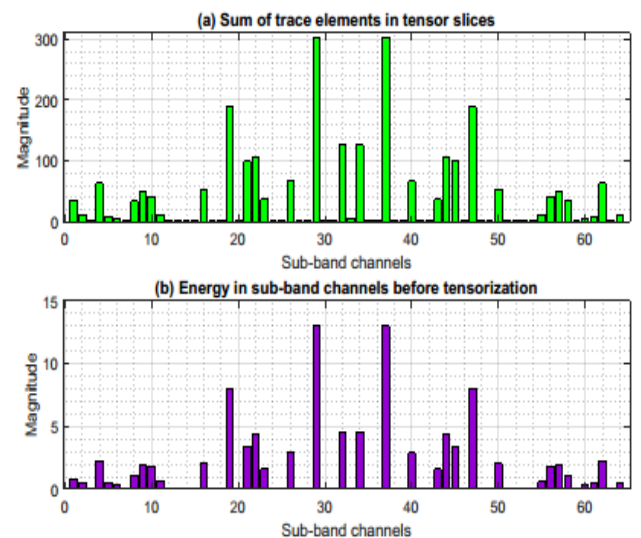

Figure 13: Profile of sum of trace elements and sub-band energy levels

The result show value of -10dB, spectrum holes were identified in 2 sub-band channels 13 and 53 from figure 14.
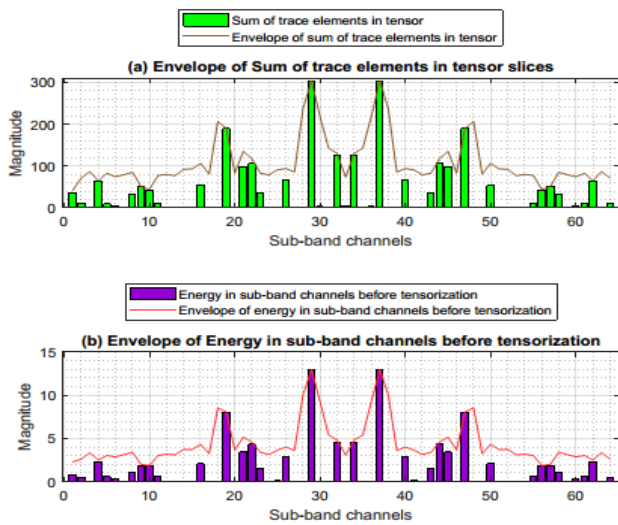

Figure 14: Envelope detection for sum of trace elements and sub-channel energies

To establish the correlation between the profile of the sum of trace elements and the energy in the sub-band channels, envelope detection is performed on the profiles in Figure 14   An observation of the two envelopes reveals that one envelope is exactly like the other, with the difference being only in magnitude.

An extraction of the envelopes as shown in Figures 15 reveals the differences in magnitude between the envelope of the sum of the trace elements in the covariance matrix in the slice of the tensor and the envelope of the energy in the sub-band channels. The relationship in (6) can be used for computing the mean of ratio of differences in magnitude or the two envelopes.

Figure 15: Extracted envelopes

From the relationship in (6), the value of the ratio is computed to be approximately 25 i.e. $ratio \approx 25$.

From the foregoing therefore, in the quest to perform spectrum hole identification, one can use the energy in the sub-band channels before tensorization or the sum of the trace elements in each covariance matrix stored as a slice of the tensor.

6 Threshold Derivation for Spectrum Hole Identification

According to Qin et al, in a time-frequency decomposition of a signal or data set such as the case of wavelet packet decomposition, the adaptive threshold for each sub-band channel based on the energy of the sub-band channel is:

$$\lambda_{i+1,2j} = \frac{\lambda_{i,j} + \alpha E_{i+1,2j}}{2} \qquad (13)$$

$$\lambda_{i+1,2j-1} = \frac{\lambda_{i,j} + \alpha E_{i+1,2j-1}}{2} \qquad (14)$$

where $\lambda_{i,j}$ is the threshold associated with the parent node, while $\lambda_{i+1,2j}$ and $\lambda_{i+1,2j-1}$ are the thresholds associated with the two sub-band channels from the parent node at the *(i+1)th* level of DWPT decomposition. $E_{i+1,2j}$ and $E_{i+1,2j-1}$ are the energies associated with the two sub-band channels at the *(i+1)th* level of DWPT decomposition. The factor α is a tuning factor in the determination of the adaptive threshold, and as it tends to 1, the

energy of the received signal has a profound effect on the adaptive threshold; if it tends to zero, the threshold at *(i+1)th* level becomes half the threshold at the *ith* level.

This work considered an FFT filterbank. As such, the parameter $\lambda_{i,j}$ in (13) and (14) will be a universal parameter since all the sub-band channels in an FFT filter bank originate from the parent node as shown in Figure 4. To derive $\lambda_{i,j}$ we propose the following problem formulation in the next section.

7 Problem Formulation using Convex Optimization

Let $x_1 \neq x_2$ be two points on ^{n} which can be expressed as:

$$y = \theta x_1 + (1-\theta) x_2 \qquad (15)$$

where $\theta \epsilon$ creates a line passing through x_1 and x_2. When $\theta = 0$, $y = x_2$; when $\theta = 1$, $y = x_1$. This implies that the value of θ between 0 and 1 corresponds to the closed line segment between x_1 and x_2.

Definition 1

A set S is convex if $\forall \theta \in [0,1]$ and $\forall u, v \in \mathbf{S}$:

$$\theta u + (1-\theta)v \in \mathbf{S}$$

If U,V $\in$ and $\theta \in [0,1]$, then $\theta u + (1-\theta)v$ is the convex combination of U and V.

Definition 2

Let $\mathbf{E}$ $\mathbb{R}^n$ be a set defined as:
$$\mathbf{E} = \{e_1, e_2, ..., e_n\}$$
$$\mathrm{E} = \{e_1, e_1, e_1, ... e_n\} \qquad (16)$$

where $e_1, e_2, ..., e_n$ are the respective sum of traces in each sub-band channel of the FFT decomposed signal. The set of all convex combinations of U and V is the set of points such that:
  $\{w_\theta \epsilon v: w_\theta = \theta + (1-\theta)v, 0 \leq \theta \leq 1\}$

Definition 3

Let e be a vector of the sum of the traces in the covariance matrices . Thus, we define e as follows:
$$\mathbf{e} = e_1, e_2, ..., e_{64} \qquad (17)$$
We define the maximum value of e in (17) as:
$\mathrm{E}_{max} = \max(e) = \max \ \mathbf{e} = \min\{e_1, e_1, e_1, ... e_n\}$
$$e_{max} = \max(\mathbf{e}) = \max\{e_1, e_2, ..., e_n\}$$
$$(18)$$
Similarly, we define the minimum value of e in (12) as:
$$e_{max} = \min(\mathbf{e}) = \min\{e_1, e_2, ..., e_n\} \quad (19)$$

Using the extrema values e_{max} and e_{min}, we can define an interval such that:
$$[e_{min}, e_{max}] \subseteq \mathbf{e} \qquad (20)$$
If we have any two points $c, d \in [e_{min}, e_{max}]$ in e such that $c < d$, then for any $\theta \in [0,1]$:
$$e_{min} \leq c = (1-\theta)c + \theta c < (1-\theta)c + \theta d < (1-\theta)d + \theta d \leq e_{max} \quad (21)$$

Also, from [21], the threshold value using the Neyman-Pearson relationship for any spectrum sensing scheme based on energy detection is given as:

$$P_f = Q\left[\left(\frac{\Gamma}{\sigma_w^2} - 1\right)\sqrt{N}\right] \qquad (22)$$

where N is the number of samples as in the DWPT sub-band channels, σ_w^2 is the noise variance with zero mean, and Γ is the threshold.

From which we obtain:

$$(\sigma_w^2)\left(\frac{Q^{-1}(P_f)}{\sqrt{N}}\right) + 1 = \Gamma \qquad (23)$$

$$\lambda_{i+1,2j-1} = \frac{\Gamma + \alpha E_{i+1,2j-1}}{2}$$

(24)

8 Performance Evaluation using Receiver Operating Characteristics (ROC)

From the performance obtained as SNR is varied from -10dB to 10dB, the Receiver Operating Characteristics ROC curve for the variation of probability of detection (P_d) with respect to probability of false alarm (P_{fa}) is shown in Figure 17. It can be seen that as SNR is varied from -10dB to 10dB, the curve becomes sharper. The confirms the increase in sensitivity to spectrum hole identification with increase in SNR.

Also, for different values of P_{fa}, the variation of P_d with respect to increase in SNR values is analyzed in the ROC curves shown in Figure 17. It can be seen at lower P_{fa}, better linearity was shown by P_d. This is what is expected of any good detection scheme.
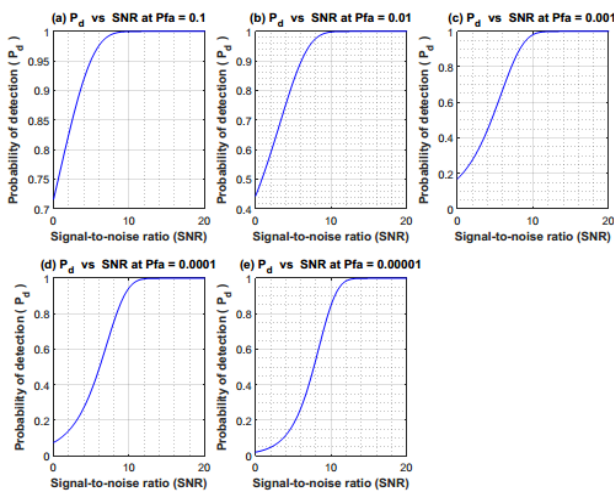

Figure 17 ROC curves for variation of P_d with respect to P_{fa}
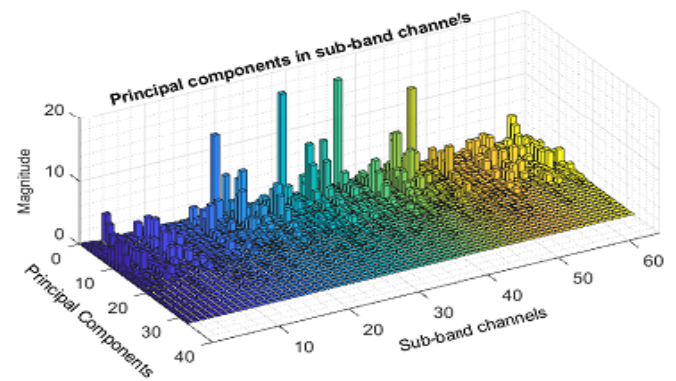

Figure 18: Principal components computed from input signal at -10dB

9 Discussion of the Result

The simulation in figure 18 shows the result of the estimated spectrum hole location is shown.

From the graph it can be deduce that the areas where the where there are no signals at all are point where noise is prevalent, while that point between 0 and 20 on the principal component axis are the point where you have high possibility of spectrum hole availability, the point between 20 and 30 on the principal axis is the point

From the coefficients in each sub-band channel, the principal components can be computed using the following steps:

Let us define a second matrix $\mathbf{Q}$ with dimension $m \times n$, and let it be associated with $\mathbf{A}$ the original input signal through a linear transformation matrix $\mathbf{Z}$ i.e. $\mathbf{QA} = \mathbf{Z}$

9.1 Measuring Performance using MSE

The results in table 1 of the performance measuring techniques is presented. The metrics of evaluating the performance of the techniques is based on the Mean Square Error (MSE) and Mean Square Error (MSE). This is given as

$$MSE = \frac{1}{n}\sum_{i=1}^{n}(Y_i - Y_{p)}^2 \qquad \ldots\ldots\ldots 24$$

MSE= 0.71621875

The results of the evaluation with respect to the measurement of the errors and closeness of measurement in terms of the MSE, RMSE Hence, an improved performance is shown in the MSE where estimated accuracy is at 84.24% for MSE and 60.31% for RMSE at SNR= 10dB,

Table 1 Evaluation of result at SNR = -10 dB

Sub-Band Channel	Trace of Tensor	Adaptive thresholding	Diff.	Sq. of Diff	Channel	Trace of Tensor	Adaptive thresholding	Diff.	Sq. of Diff.	Channel	Trace of Tensor	Adaptive thresholding	Diff.	Sq. of Diff
1	53	51	-3	9	22	120	100	-20	400	43	49	40	-23	529
2	27	25	-2	4	23	42	40	-7	49	44	120	100	-35	1225
3	20	20	2	4	24	5	5	0	0	45	138	115	70	4900
4	80	70	-15	225	25	10	10	0	0	46	40	40	0	0
5	22	22	-2	4	26	80	77	-10	100	47	170	140	-10	100
6	19	19	-2	4	27	10	16	0	0	48	20	20	0	0
7	18	18	2	4	28	5	5	0	0	49	40	40	3	9
8	52	45	-3	9	29	295	240	-60	3600	50	70	60	-4	16
9	80	70	-10	100	30	10	10	0	0	51	22	22	1	1
10	68	58	-9	81	31	10	15	0	0	52	22	24	0	0
11	39	32	-2	4	32	141	120	-30	900	53	30	40	0	0
12	22	24	0	0	33	38	37	0	0	54	26	35	2	4
13	21	26	1	1	34	145	121	-30	900	55	36	31	-1	1
14	20	23	0	0	35	7	9	0	0	56	68	56	-12	144
15	21	21	1	1	36	8	8	0	0	57	70	58	-11	121
16	70	6	-10	100	37	290	240	-60	3600	58	55	48	-4	16
17	5	5	0	0	38	10	10	0	0	59	18	12	0	0
18	5	5	0	0	39	20	19	0	0	60	40	41	0	0
19	170	140	-30	900	40	80	70	-10	100	61	42	40	-1	1
20	3	3	0	0	41	10	10	0	0	62	80	60	-10	100
21	130	110	-20	400	42	5	5	0	0	63	40	37	0	0

10 Conclusion

The paper worked on Using Covariance Matrix and Fast Fourier Transform for Estimating Spectrum Hole Location in Cognitive Radio Network It developed an enhanced technique which first used Fast Fourier Series Transform to split the Spectrum into sub-band channels. Covariance Marix was used in determining the actual range for the bounds,64 sub-band decomposition was achieved also using Fast Fourier Transform (FFT), It showed that there exists a relationship between the covariance matrix and the sub-band energy, the performance obtained as SNR is varied from -10dB to 10dB, the Receiver Operating Characteristics ROC curve for the variation of probability of detection (P_d) with respect to probability of false alarm (P_{fa}) is discovered. It can be seen that as SNR is varied from -10dB to 10dB, the curve becomes sharper. The confirms the increase in sensitivity to spectrum hole identification with increase in SNR.

References

[1] J. Jacob, "Spectrum Prediction In Cognitive Radio Networks : A Bayesian Approach," in Eighth International Conference on Next Generation Mobile Applications, Services and Technology,, 2014.

[2] K. Benghabrit Nawel, ""Optimizing the Capacity Of Cognitive Radio Networks With Power Control And Variable Spectrum Allocation," Transport and Telecommunication, vol. 19, no. no 2, pp. pp 128 - 139, 2018.

[3] S. Raghave, "Continuous Wavelet Transform Based Spectrum Sensing in Cognitive Radio," Research Journal of Applied Sciences, Engineering and Technology, vol. VOL 7, no. 5, pp. pp 986-988, 2018.

[4] J. Agajo, O. Joseph, S. E. Ezewele, and A. Theophilus(2011) Spatial Analysis of Signal Strength in a Wireless Communication Medium for Indoor Geolocation System International Journal of Computer Theory and Engineering, Vol. 3, No. 4, August Singapore pp502-508 available online at http://www.getcited.org/pub/103485556

[5] S. Ahmed, " Eng. Centre For Telecommunications And Micro-Electronics," Faculty Of Health, Engineering And Science,Victoria University: Engineering And Science,Victoria University.

[6] S. Nadir Hussin, ""United Arab Emirates University Scholarworks@UAEU," Spectrum Sharing In Cognitive Radio Networks With Quality Of Service Awareness," 2011.

[7] M. McHenry, ""Proceedings of the First International Workshop on Technology and Policy for Accessing Spectrum, ser. TAPAS '06. ACM in Accessing Spectrum, ser. TAPAS '06," New York, 2006.

[8] A. Wisniewska, "A white paper on spectrum sharing," 2012.

[9] Y. Adeel Ahmed, "Noise Variance Estimation for Spectrumss Sensing in Cognitive Radio Networks," in in Conference on Circuit and Signal Processing (CSP 2014), AASRI, 2014.

[10] T. Huseyin, " A Survey of Spectrum Sensing Algorithms for Cognitive Radio Applications," IEEE communications surveys & tutorials , vol. VOL 11, no. 1, 2009.

[11] H. Tevfik Yucek, "A Survey of Spectrum Sensing Algorithms for Cognitive radio Application," IEEE Communication Survey and Tutorials, vol. vol 11, no. 1, 2009.

[12] James Agajo, : Isaac O. Avazi Omeiza,: Idigo Victor Eze, : Okhaifoh Joseph(2011) Dynamic Approach to Enhanced Performance of Orthogonal Division Multiplexing (OFDM) in a Wireless Communication Network, International Journal of advance Computer Studies and application (Vol. 2 Issue 2) New York(U.S.A) , pp58-68 available online at http://thesai.org/Publications/ViewPaper?Volume=2&Issue=2&Code=IJACSA& SerialNo=11

[13] H. Mohammed Mehdi Saleh, ""Quick Detection and Assignment of Spectrum Hole in Cognitive Radio," in in International conference on Intelligent Systems, Data Mining and Information Technology (ICIDIT'2014), 2014.

[14] T. Xiaowen Gong, " Joint bandwidth and `power allocation in wireless multi-user decode-and-forward relay networks," in in Conference: Proceedings of the IEEE International Conference on Acoustics, Speech, and Signal Processing, Dallas, 2014.

[15] Coye, A. Haskelkorn and S. Demello, "Remote Patient Management: Technology-Enabled Innovation and Evolving Business Models for Chronic Disease Care, Health Affairs," 2009.

[16] Farah and Abdellatif, "Smart Mobile Healthcare System based on WBSN, and 5G," International Journal of Advanced Computer Science and Applications, vol. Vol 8, no. No. 10, 2017.

[17] J. Agajo, N. Bello, F. Ntekim, O. B. Chukwuejekwu and L. O. Uzoechi, "ZigBee based

wireless patient temperature and pulse monitoring system," Journal of Wireless Sensor Networks, vol. vol 3, no. no. 3, 2016.

[17]   J. Agajo, G. Jonathan kolo, I. Obiora-Dimson, O. B. Chukwueze and O. Lazarus Uzoechi, ""Remote monitoring and automated diagnosis via interactive sofware interface using wireless communication network," Journal of Science, Technology & Education (JOSTE), vol. Vol 4, no. No. 1, 2016.

[18]   Kakria, Tripahithi and Kitipawang, ""A Real-Time Health Monitoring System for Remote Cardiac Patients Using Smartphone and Wearable Sensors," International Journal of Telemedicine and Applications, vol. Vol 15, p. pp. 11, 2015.

[19]   J. Agajo, G. Jonathan kolo, I. Obiora-Dimson, O. B. Chukwueze and O. Lazarus Uzoechi, ""Remote monitoring and automated diagnosis via interactive sofware interface using wireless communication network," Journal of Science, Technology & Education (JOSTE), vol. Vol 4, no. No. 1, 2016.

[20]   A. Kala Venugopal, "Centralized Heart Rate Monitoring and Automated Message Alert System using WBAN," International Journal of Scientific and Research, vol. Vol 3, no. issue 9, 2013.

[21]   M. Aminian and H. R. Naji, "A Hospital Healthcare Monitoring System Using Wireless Sensor Networks," Journal of Health & Medical Informatics, vol. Vol 4, no. No 2, 2013.

[22]   P. Sundaram, "Patient monitoring system using android technology," International Journal of Computer Science and Mobile Computing, vol. Vol 2, no. Issue 5, pp. pp. 191-201, 2013.